Journal of Volcanology and Geothermal Research 206 (2011) 136–147

Contents lists available at ScienceDirect

Journal of Volcanology and Geothermal Research

journal homepage: www.elsevier.com/locate/jvolgeores

A reconnaissance of U-Pb zircon ages in the Cerro Galán system, NW Argentina: Prolonged magma residence, crystal recycling, and crustal assimilation

Chris B. Folkes [a,*], Shanaka L. de Silva [b], Axel K. Schmitt [c], Raymond A.F. Cas [a]

[a] School of Geosciences, P.O. Box 28E, Monash University, Clayton, VIC 3800, Australia
[b] Department of Geosciences, Oregon State University, Corvallis, OR 97331, USA
[c] Department of Earth and Space Sciences, University of California, Los Angeles, 595 Charles Young Dr., Los Angeles CA, 90095-1567, USA

ARTICLE INFO

Article history:
Received 13 July 2010
Accepted 8 June 2011
Available online 28 June 2011

Keywords:
$^{206}Pb/^{238}U$
Antecrysts
Xenocrysts
Crystal-rich ignimbrites
Magma residence times

ABSTRACT

$^{206}Pb/^{238}U$ ages obtained from Secondary Ionization Mass Spectrometry (SIMS) analyses of zircon crystals in eight ignimbrites from Cerro Galán (Central Andes) reveal insights into magma dynamics and crystallization histories of a sustained (>3.5 Ma), large-volume, crystal-rich magmatic system. This makes the Galán volcanic system an excellent example of repeated large-volume ignimbrite eruptions from a single magmatic system with eruptive recurrence intervals between ~50 ka and possibly >1 Ma. $^{40}Ar/^{39}Ar$ sanidine and biotite ages indicate eruption ages between ~2.0 and 5.6 Ma, although biotite results are likely affected by extraneous ^{40}Ar. In each ignimbrite, interiors of zircon *autocrysts* frequently crystallized up to several 100's ka prior to eruption, consistent with long upper-crustal residence times of the pre-eruptive Galán magmas. Many ignimbrites also contain zircon *antecrysts* that crystallized in the preceding cycle in the Galán eruptive sequence. Finally, rare (~540 to 500 Ma) zircon *xenocrysts* are also present, derived from basement rocks that comprise the regional upper crust into which the Galán magmas intruded. In some cases, near eruption-age zircon has overgrown xenocrysts and antecryst cores. We infer that silicic magmas were repeatedly intruded into the shallow crust, whereby antecrysts became recycled from non-erupted progenitors to the earlier ignimbrite eruptions. Complex crystal populations observed in the Galán Ignimbrites are consistent with those detected in other large 'monotonous' ignimbrites, but Galán differs from many other silicic systems in that it represents a well-preserved system that frequently tapped silicic magma from the same long-lived spatially-focused system. The magma dynamics revealed by our reconnaissance zircon geochronology are consistent throughout the magmatic cycles at Galán and are independent of eruptive volume: pre-eruptive zircon crystallization within <500 ka prior to eruption, with episodic recycling of non-erupted material of older eruptions and assimilation of crustal material local to the region.

1. Introduction

The processes involved in the growth of large silicic magma chambers are inherently complex. Chemical and physical evolution of magma chambers include a combination of fractionation, assimilation, and punctuated mafic recharge processes (e.g., Smith, 1979; Hildreth, 1981; Bachmann et al., 2002). The timescales necessary to reach eruptible large volumes vary between different centers, and range between 10^3 and 10^6 yr as estimated from repose intervals between eruptions (White et al., 2006). Magma accumulation timescales have also been estimated from the difference between the ages of eruption and crystallization that can amount to pre-eruptive crystal residence times of 10^5 yr (Simon et al., 2008). In some cases, crystal residence times vary depending on the volumes and repose intervals between eruptions. Where repose intervals are short, ($<10^4$ yr), corresponding crystal residence times are also short ($<10^4$ yr; e.g., the 27 ka, 530 km^3 Oruanui Ignimbrite, New Zealand, Wilson and Charlier, 2009; the 760 ka, 650 km^3 Bishop Tuff, California, Reid and Coath, 2000; Simon and Reid, 2005; and post-caldera deposits at Yellowstone, USA, Bindeman et al., 2008). This is in contrast to extremely large-volume silicic eruptions where repose intervals are longer ($>10^5$ yr), with the opportunity for subsequent crystal residence times $>10^5$ yr (e.g., the 28 Ma, 5000 km^3 Fish Canyon Tuff, Bachmann et al., 2007b; the 340 ka, >1000 km^3 Whakamaru group ignimbrites, New Zealand, Brown and Fletcher, 1999; and ignimbrites from the La Pacana caldera, Schmitt et al., 2002).

Crystals contained within juvenile clasts of large-volume pyroclastic deposits provide valuable information about the nature of their magmatic systems prior to eruption. Eruptions of this type eviscerate the tops of granite batholith-scale magmas at an instant in their evolution, providing a vital window into processes within the plutonic

* Corresponding author. Tel.: +61 423205746; fax: +61 399054903.
E-mail addresses: chris.folkes@monash.edu (C.B. Folkes), desilvas@geo.oregonstate.edu (S.L. de Silva), axel@oro.ess.ucla.edu (A.K. Schmitt), ray.cas@monash.edu (R.A.F. Cas).

0377-0273/$ – see front matter © 2011 Elsevier B.V. All rights reserved.
doi:10.1016/j.jvolgeores.2011.06.001

system (Lipman, 1984). Thus the resultant large-volume crystalline felsic ignimbrites, often termed 'monotonous intermediates' (e.g., Smith, 1979; Hildreth, 1981) are thought of as the surface expressions of 'monotonous plutons' or magma chambers that are not zoned or only weakly zoned (e.g., Whitney and Stormer, 1985; de Silva and Wolff, 1995).

Magmatic crystals can be divided into three main populations (e.g., Schmitt, 2011): (1) *phenocrysts* (or *autocrysts* if size does not permit unaided visual identification) that crystallized directly from the accumulating magma associated with a particular eruption; (2) *antecrysts* (or *phoenicrysts* if there are significant hiatuses between recurrent crystallization intervals) incorporated from previous crystallization events within the same magmatic system; and (3) *xenocrysts* incorporated from the wall-rocks as the magma was generated, grew, migrated and accumulated in the crust prior to eruption. Xenocrysts are common in some large silicic ignimbrites (e.g., Charlier et al., 2005) that are inferred to contain large amounts of crustal material (based on Nd, Sr and O-isotope data). Distinguishing phenocrysts from antecrysts within large silicic ignimbrite magmas can be more challenging. Where a magmatic system has erupted multiple magmas with distinctive chemistries, these different crystal types can often be identified based on trace element and isotopic fingerprinting that corresponds to a particular magma batch (e.g., Charlier et al., 2007). In contrast, where successive erupted magmas have nearly identical isotopic signatures and similar major, minor, and trace element chemistries, distinctions between phenocrysts and antecrysts can be more cryptic and require geochronological analyses (Bacon and Lowenstern, 2005). This is particularly true for the large volume, chemically 'monotonous' crystal-rich ignimbrites from the Altiplano-Puna Volcanic Complex (APVC, e.g., de Silva, 1989a; de Silva, 1989b; Lindsay et al., 2001), and the Cerro Galán Ignimbrites (e.g., Francis et al., 1989) of the Central Andes, as well as the Fish Canyon Tuff (e.g., Bachmann et al., 2007b) and the Lund Tuff (Maughan et al., 2002) of the Great Basin, USA.

In these cases, U-Pb zircon geochronology is a useful tool in identifying different crystal populations that can be obscured by the general chemical homogeneity of magma batches. Zircon is ubiquitous in felsic ignimbrites and resistant to diffusion even at elevated temperatures, as illustrated by the preservation of intricate zonations in trace element contents that can be imaged via cathodoluminescence (Cherniak and Watson, 2003). Dating is aided by high partition coefficients for uranium (~100; Mahood and Hildreth, 1983; Blundy and Wood, 2003) that permits U-decay-based geochronology. Recognizing the presence and relative proportions of different zircon populations at sub-grain domain scales thus allows inferences about magma genesis, interaction with crustal-material and magmatic progenitors, storage times in shallow chambers just prior to eruption, and changes in magmatic conditions such as temperature, pressure and volatile contents (e.g., Reid et al., 2011).

Here we report the results of an investigation of the pre-eruptive crystallization histories of zircon crystals beneath the Cerro Galán caldera system in NW Argentina; a long-lived, spatially-focused, crystal-rich silicic volcanic system with a well-constrained stratigraphy that evolved to supervolcanic proportions at the climax of its >3.5 Ma history (Sparks et al., 1985; Folkes et al., 2011a). We show that ion microprobe $^{206}Pb/^{238}U$ ages of zircon crystals from multiple ignimbrites at Cerro Galán clearly identify different crystal populations (autocrysts, antecrysts, and xenocrysts) and their relative abundances in successive ignimbrite eruptions at Cerro Galán, whereas micro-chemical characterization of crystal populations using micro-chemical techniques remains inconclusive (e.g., Folkes et al., 2011b). The difference between U-Pb zircon autocryst ages and the $^{40}Ar/^{39}Ar$ eruption age for a given ignimbrite magma is then used to infer the length and nature of the crystallization history of zircon, and therefore the magma, prior to eruption of the Galán Ignimbrites.

2. The Cerro Galán caldera

2.1. Geologic setting and ignimbrite stratigraphy

The Cerro Galán caldera volcano in NW Argentina (Fig. 1a) lies on the Puna, an elevated plateau with elevations of 3500 to 6000 m above sea level and a crustal thickness of 55–60 km (Sparks et al., 1985; Kay and Coira, 2009). Cerro Galán has erupted at least nine medium to large volume silicic ignimbrites, all high-K, crystal-rich

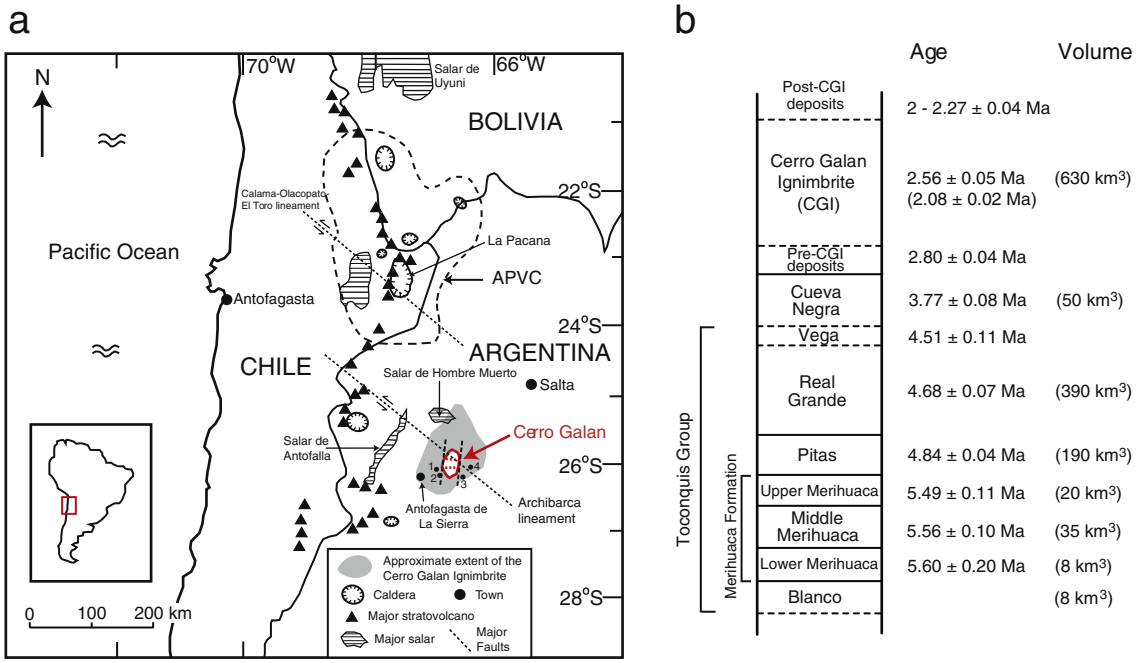

Fig. 1. (a) Location of the Cerro Galán caldera and surrounding features. Locality information: 1. Rio de Las Pitas; 2. Rio Pirica; 3. Rio Leon Muerto; 4. Headwaters of Rio de Los Patos. (b) Stratigraphy of the Galán ignimbrites and their associated $^{40}Ar/^{39}Ar$ biotite ages and erupted volumes (a $^{40}Ar/^{39}Ar$ sanidine age for the CGI is shown in parentheses; from Folkes et al., 2011a).

(40–50% crystals on a vesicle-free basis), and chemically homogeneous rhyodacites (SiO_2 = 68–71 wt.%), with little variation in bulk-rock and mineral chemistries (Folkes et al., 2011b). Ignimbrite activity commenced at ~6 Ma (K-Ar methods, Sparks et al., 1985). Folkes et al. (2011a) provide new $^{40}Ar/^{39}Ar$ dates, an updated stratigraphy and volume estimates for the Galán Ignimbrites (Fig. 1b). Basement outcrops in this area consist of Late Neoproterozoic Pachamama and Rio Blanco Formations and early Ordovician granites and granodiorites (~600 to 420 Ma by K-Ar analyses, Sparks et al., 1985; Hongn and Seggiaro, 2001). Small-volume, dacitic lava flows have been dated ~9 to 10 Ma (Francis et al., 1980) although caldera-forming activity in this region may have started much earlier, >12 Ma (Sparks et al., 1985; Guzman and Petrinovic, 2010). The earliest erupted ignimbrites comprise the Toconquis Group and consist of the Blanco Ignimbrite (age unknown, 8 km^3), Lower, Middle and Upper Merihuaca Ignimbrites (5.60–5.49 Ma, 8–35 km^3 Dense Rock Equivalent, DRE), the Pitas Ignimbrite (4.84 ± 0.04 Ma, ~190 km^3 DRE), the Real Grande Ignimbrite (4.68 ± 0.07 Ma, ~390 km^3 DRE) and the Vega Ignimbrite (4.51 Ma, volume unknown; Fig. 1b). There was then a hiatus of ~0.75 Ma until the eruption of the Cueva Negra Ignimbrite (3.77 ± 0.08 Ma, ~50 km^3 DRE) with a period of quiescence of ~1–2 Ma that was followed by the voluminous 2.08 ± 0.02 Ma (Kay et al., 2011; Hora et al., 2011) eruption of the ~630 km^3 Cerro Galan Ignimbrite (CGI) with associated pre-CGI domes and lavas (2.80 Ma) and post-CGI domes, surges and small-volume ignimbrites (2.00–2.27 Ma, Fig. 1b).[1] The eruption of the CGI facilitated caldera collapse, producing the volcano-tectonic depression observed today (see Folkes et al., 2011a) for a more detailed account of the stratigraphy and volcanology of the Galán system.

2.2. Juvenile clast types

Two main types of juvenile clasts are present throughout the Galán Ignimbrites. By far the most common type is 'white' pumice. It accounts for ~95% by volume of all juvenile clasts and is characterized by its color, high content of large (up to 8 mm diameter) crystals (up to 55 volume% on a vesicle-free basis) and generally large vesicles (Folkes et al., 2011b). 'Gray' pumice clasts are also found throughout the Galán ignimbrite stratigraphy, but account for only ~5% by volume of the juvenile clast proportion. They are denser with a finer-grained crystal and vesicle texture. The physical differences between these juvenile clast types are related to textural differences in vesicle size and the presence (gray pumice) or absence (white pumice) of microlites (Wright et al., 2011). The white pumice corresponds to large-volume rhyodacitic magma that resided at shallow depth in this tectonic setting (~8 to 1.5 km; Al-in-hornblende barometry, Folkes et al., 2011b). Each magma body in the Galán system is shown to have originated from a common 'parent' magma (represented by gray pumice clasts present in the CGI) that originated at slightly deeper levels (>15 km; Al-in-hornblende barometry) with higher temperatures (Fe-Ti oxide thermometry, Folkes et al., 2011b). These magmas subsequently ascended, mingled with, and possibly provided the eruption trigger to the more voluminous white pumice magmas in shallow chambers (Wright et al., 2011). A corollary relationship between the white and gray pumice in the 4.09 Ma, 1500 km^3 Puripicar Ignimbrite of the APVC has been identified by de Silva and Francis (1989) and de Silva (1991), implying similar magmatic histories for these two supervolcanic systems in the Central Andes.

Preliminary data from melt inclusions trapped within quartz crystals show no systematic difference in water contents across the temporal history of the Galán Ignimbrites (all pumice clasts in ignimbrites generally contain a range of 2–5 wt.% H_2O, Wright et al., 2011 and unpublished data).

Coupled with very consistent major and trace elements (in both the white and gray pumice clast population) and isotopic characteristics that implicate broadly similar magma genesis and dynamics, there are some subtle, but significant variations in minor and trace elements in dominant white pumice clasts between the Galán Ignimbrites (Folkes et al., 2011b). Variations in bulk-rock concentrations of Nb, Ta, Y and Yb suggest variable amounts of upper-crustal crystal fractionation from a common gray pumice parent magma (Folkes et al., 2011b), with the larger volume CGI and Real Grande Ignimbrites recording slightly less crystal fractionation than the earlier, smaller volume Toconquis Group magmas. Evidence from phenocryst compositions and proportions show that the younger sanidine-bearing ignimbrites erupted from the Galán system (the Cueva Negra and CGI) crystallized at slightly shallower depths than the older amphibole-bearing Toconquis Group Ignimbrites.

3. Sample selection and analytical methods

Only dominant white pumice blocks from each ignimbrite were used for this study. Samples from the Toconquis Group Ignimbrites (except for the Vega Ignimbrite) were collected to the SW of the caldera (at Rio de Las Pitas and Rio Pirica; ~12 km and 10 km from the western structural margin, respectively; Fig. 1a). Pumice clasts from the Cueva Negra Ignimbrite were sampled from Rio Leon Muerto, ~10 km from the southeastern structural margin (Fig. 1a). Pumice clasts from the CGI were sampled from near the headwaters of Rio de Los Patos, ~20 km from the eastern structural margin (Fig. 1a).

Bulk pumice samples were crushed using a hydraulic press and a disk mill. The crushed samples were then processed using heavy liquid and magnetic separating methods. Between five and ten zircon crystals were selected per sample (except for the Lower Merihuaca and Blanco Ignimbrites where <5 crystals were available). Two samples were processed for each of the Cueva Negra and Upper Merihuaca Ignimbrites. Zircon crystals were selected at random from the bulk separates with no preference given to size or morphology. Crystal sizes ranged from 60 to 250 μm in length. Upon inspection, there were no noticeable morphological variations between crystals and the entire population was of a pink-red color. Zircon crystals were cleaned with acetone and mounted in epoxy resin, sectioned to expose grain interiors and polished with 1 μm Al_2O_3. After ultrasonic cleaning, grains were surveyed for internal compositional zonations and/or inclusions via cathodoluminescence (CL) imaging using a Leo 1430VP scanning electron microscope at UCLA (e.g., Fig. 2). U, Th, and Pb isotopic measurements were obtained using the UCLA CAMECA ims 1270 ion microprobe. Samples that had been coated with ~10 nm of Au were probed with a mass-filtered, 10–20 nA $^{16}O^-$ beam focused to a ~30–35 μm diameter spot. Secondary ions were extracted at 10 kV with an energy band-pass of 50 eV. The mass spectrometer was tuned to a mass resolution of ~5000 to resolve molecular interferences in the mass range analyzed ($^{94}Zr_2O^+$, $^{204}Pb^+$, $^{206}Pb^+$, $^{207}Pb^+$, $^{208}Pb^+$, $^{238}U^+$, $^{232}Th^{16}O^+$, $^{238}U^{16}O^+$). Flooding the analysis surface with O_2 at a pressure of ~4×10^{-3} Pa increased Pb^+ yields by nearly a factor of 2. The relative sensitivities for Pb and U were determined on reference zircon *AS3* (Paces and Miller, 1993) using a calibration technique similar to Compston et al. (1984). Th and U contents (uncertainties ~10%) were estimated by multiplying measured $^{232}Th^{16}O^+/^{94}Zr_2O^+$ and $^{238}U^{16}O^+/^{94}Zr_2O^+$ ratios on the unknowns with corresponding relative sensitivity values determined on reference zircon *91500* (Th = 28.6 ppm; U = 81.2 ppm; Wiedenbeck et al., 1995). Target surfaces were pre-sputtered for 4 min before analysis to minimize surface Pb contamination. $^{206}Pb/^{238}U$ age uncertainties at high radiogenic yields are ~5% (i.e., ±0.1 Ma for the

[1] $^{40}Ar/^{39}Ar$ biotite ages may not reflect accurate 'eruption' ages in the Galán Ignimbrites. For example, The 2.27 Ma $^{40}Ar/^{39}Ar$ biotite age for a post-CGI deposit is older than the 2.08 Ma $^{40}Ar/^{39}Ar$ sanidine age for the CGI. This is due to problems with extraneous ^{40}Ar contained within biotite crystals. For a more detailed discussion, see Section 5.1.

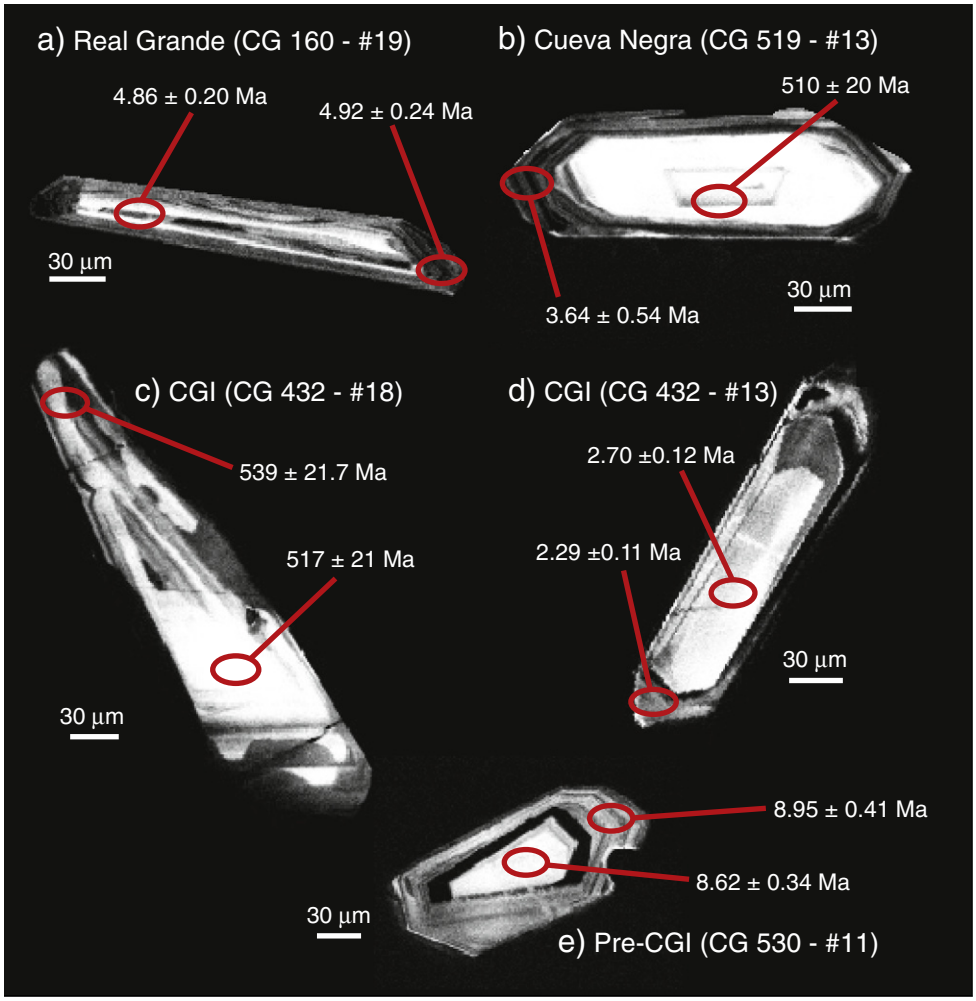

Fig. 2. Selected cathodoluminescence (CL) images of zircon crystals from: (a) the Real Grande Ignimbrite, (b) the Cueva Negra Ignimbrite, (c) and (d) the Cerro Galán Ignimbrite (CGI), (e) Pre-CGI. Analyzed spots with their corresponding $^{206}Pb/^{238}U$ ages (by SIMS) are shown with ±1 sigma uncertainties.

youngest ignimbrites in the Galán system). Spot analyses on low uranium zircons, or those that accidentally overlap with common Pb bearing phases such as glass or apatite, have higher uncertainties. Values for common Pb corrections are taken from Sanudo-Wilhelmy and Flegal (1994).

4. Results

Table 1 and Fig. 3a (Tera–Wasserburg diagrams) present $^{207}Pb/^{206}Pb$ and $^{206}Pb/^{238}U$ ion microprobe data for 104 interior and rim analyses from 54 zircon crystals analyzed in this study. Fig. 3b presents probability density plots and associated histograms for each ignimbrite generated with the Isoplot/Ex 3.00 software (Ludwig, 2003).

The majority of zircon analyses within each ignimbrite yield ages that overlap within error (±1 sigma), forming a strong normal distribution (open bars in Fig. 3b). These crystals show a continuous age range (accounting for the ±1 sigma uncertainties in U-Pb analyses), whereby the difference between the youngest and oldest individual zircon age within a clustering group of ages is up to 0.94 ± 0.33 Ma (an average of 0.64 ± 0.26 Ma), typically in excess of the averaged age uncertainty (0.27 Ma, ±1 sigma) of all individual spot analyses in this population (Table 1). Most zircon crystals in this first population (population 1) show no discernable variation in ages within lateral dimensions of the ion beam targeting near-rim and near-core domains of the sectioned crystals. For example, crystal #19 of CG 160 (the Real Grande Ignimbrite) yields an interior age of 4.86 ± 0.20 Ma and a rim age of 4.92 ± 0.24 Ma (Fig. 2a). The remainder of zircon ages falls into two main populations. The second population (population 2), present in the Lower Merihuaca, Cueva Negra, pre-CGI Ignimbrites and the CGI, contain ages that correspond (within error) to the main zircon crystallization age range (as described above) of each preceding ignimbrite in the Galán stratigraphy (light gray bars in Fig. 3b). For example, crystal #10 in the Real Grande Ignimbrite (sample CG 160) yields interior and rim ages that correspond to the main zircon age range of the underlying Upper Merihuaca Ignimbrite (Fig. 3b). There are also older zircon ages in this second population. A single zircon crystal (CG 530; crystal #11) yields overlapping U-Pb ages of 8.62 ± 0.34 Ma (interior) and 8.95 ± 0.41 Ma (rim; Fig. 3b). These ages are >2.5 Ma older than zircon crystals from the lowermost ignimbrite in the Galán stratigraphy, the Blanco Ignimbrite. The CGI, pre-CGI, Cueva Negra and Lower Merihuaca Ignimbrites contain a third zircon population (population 3), consisting of analyses with much older U-Pb ages of 504 ± 23 to 539 ± 22 Ma, (Table 1 and Figs. 2c, 3b), typical for local basement rocks in which the modern Galán system developed (Sparks et al., 1985).

Some zircon crystals also contain interiors and rims with analytically distinguishable U-Pb ages (Figs. 2b, d). This zircon age zonation, with younger rim overgrowths on older interiors, is present in crystals in the CGI and Cueva Negra Ignimbrite (Figs. 2b, d). For example, crystal #16 in the Cueva Negra Ignimbrite (sample CG 436) yields an interior age of 4.58 ± 0.31 Ma and a rim age of 3.49 ± 0.15 Ma (Table 1). The age yielded by this zircon rim is within error of

Table 1
SIMS U-Pb zircon results of the Galán Ignimbrites.

[a]Ignimbrite $^{40}Ar/^{39}Ar$ age [Ma]	Sample and crystal number	Core/rim analyses	$^{238}U/^{206}Pb$	$^{238}U/^{206}Pb$ 1 s.e.	[b] $^{207}Pb^*/^{206}Pb^*$ 1 s.e.	$^{207}Pb^*/^{206}Pb^*$ 1 s.e.	Correlation of concordia ellipses	Radiogenic %	U ppm	Th ppm	$^{206}Pb/^{238}U$ Age t [Ma]	1 sigma t [Ma]	[c] Δt [Ma]
Cerro Galan Ignimbrite (CGI) 2.08 ± 0.02	CG432_13	R	2860	136	0.069	0.004	0.05	97.1	3000	610	2.29	0.11	0.21
	CG432_14	C/R	2850	147	0.109	0.012	0.05	91.9	1000	540	2.16	0.12	0.08
	CG432_15	C/R	2560	104	0.056	0.003	0.04	98.7	4400	1200	2.59	0.10	0.51
	CG432_2	C	2790	129	0.079	0.004	−0.09	95.8	2800	1100	2.31	0.11	0.23
	CG432_2	C	2810	121	0.058	0.004	−0.08	98.4	4400	1800	2.35	0.10	0.27
	CG432_3	C	2790	127	0.078	0.006	0.20	95.9	1900	300	2.31	0.11	0.23
	CG432_3	R	2670	122	0.124	0.009	−0.12	90.0	1300	770	2.26	0.12	0.18
	CG432_5	C	2650	117	0.079	0.007	0.10	95.8	2100	360	2.43	0.11	0.35
	CG432_5	R	2770	126	0.072	0.006	−0.25	96.7	2900	800	2.35	0.11	0.27
										Average	2.35	0.07	
										MSWD		1.17	
	CG432_13	C	2400	107	0.071	0.005	−0.01	96.8	2700	460	2.70	0.12	0.62
	CG432_13	C	2340	147	0.057	0.003	−0.02	98.7	3800	540	2.82	0.17	0.74
	CG432_18	C	12.0	0.5	0.058	0.000	0.01	99.9	790	73	517	21	515
	CG432_18	R	11.5	0.5	0.059	0.001	0.02	99.9	520	93	539	22	536
Pre-CGI 2.80 ± 0.04	CG530_16	C/R	2490	110	0.065	0.003	−0.09	97.5	4600	890	2.63	0.12	
	CG530_1	R	2500	112	0.083	0.008	−0.09	95.3	1100	350	2.55	0.12	
	CG530_1	C	2410	124	0.061	0.004	−0.06	98.0	2400	710	2.71	0.14	
	CG530_2	R	2750	146	0.065	0.006	0.05	97.6	2100	930	2.38	0.13	
	CG530_2	C	2700	145	0.059	0.005	0.02	98.3	3700	1600	2.44	0.13	
	CG530_7	C	2190	136	0.105	0.008	0.39	92.4	2000	970	2.81	0.19	
	CG530_7	R	2620	133	0.055	0.003	0.19	98.8	3900	1000	2.53	0.13	
	CG530_8	C	1870	158	0.330	0.051	−0.19	63.4	240	260	2.24	0.39	
										Average	2.55	0.10	
										MSWD		1.00	
	CG530_11	C/R	741	28.8	0.060	0.002	−0.01	98.2	3000	1300	8.62	0.34	
	CG530_11	R	721	33.0	0.053	0.002	0.04	99.1	3000	810	8.95	0.41	
	CG530_5	C	11.8	0.6	0.058	0.000	0.03	100.0	700	85	525	24	
	CG530_5	R	12.0	0.6	0.059	0.001	−0.01	99.8	630	98	517	24	
Cueva Negra 3.77 ± 0.08	CG436_1	C/R	1630	76.6	0.061	0.004	0.02	98.0	1900	430	3.97	0.19	
	CG436_16	R	1840	77.3	0.072	0.004	−0.02	96.7	2200	330	3.49	0.15	
	CG436_2	C/R	1700	74.2	0.058	0.004	0.03	98.5	1900	760	3.83	0.17	
	CG436_3	C/R	1830	86.1	0.066	0.006	0.10	97.5	2700	510	3.53	0.17	
	CG436_7	C/R	1780	76.3	0.064	0.004	0.06	97.7	2200	370	3.64	0.16	
	CG436_7	R	808	61.5	0.464	0.018	−0.17	46.2	2500	760	3.78	0.76	
	CG436_8	C/R	1440	69.3	0.128	0.011	−0.21	89.5	2900	790	4.11	0.23	
										Average	3.71	0.21	
										MSWD		1.50	
	CG436_16	C	1280	77.0	0.130	0.009	0.11	89.2	1200	290	4.58	0.31	
	CG436_23	C/R	1280	43.8	0.050	0.002	−0.06	99.5	10,400	7700	5.07	0.17	
	CG519_13	R	548	20.1	0.589	0.008	0.00	30.1	4900	1100	3.64	0.54	
	CG519_15	C	1470	72.2	0.066	0.003	−0.05	97.4	1900	3700	4.29	0.22	
	CG519_15	R	754	37.7	0.475	0.020	−0.27	44.9	4000	490	3.94	0.59	
	CG519_19	C	1580	86.8	0.058	0.004	−0.03	98.5	3800	820	4.11	0.22	
	CG519_19	R	1740	73.0	0.087	0.006	−0.09	94.7	4000	760	3.61	0.17	
	CG519_20	C	1790	121	0.085	0.012	−0.23	95.0	580	460	3.50	0.25	
	CG519_20	R	1690	113	0.090	0.009	−0.28	94.3	670	510	3.68	0.26	
	CG519_3	C	1760	137	0.086	0.009	−0.08	94.8	540	570	3.53	0.29	
	CG519_3	R	1670	125	0.089	0.012	0.03	94.5	570	610	3.70	0.29	
	CG519_7	C	1610	131	0.169	0.033	−0.19	84.2	260	390	3.42	0.38	
	CG519_7	R	1590	170	0.190	0.036	−0.31	81.5	150	190	3.35	0.49	
	CG519_9	C	1420	117	0.119	0.019	−0.07	90.6	400	230	4.19	0.39	
	CG519_9	R	1750	110	0.082	0.007	−0.05	95.4	710	470	3.58	0.23	
										Average	3.76	0.18	
										MSWD		1.20	
	CG519_13	C	12.2	0.5	0.058	0.000	0.00	100.0	610	390	510	20	
Real Grande 4.68 ± 0.07	CG160_11	C	1260	60.2	0.067	0.004	−0.01	97.3	2100	440	5.06	0.25	
	CG160_16	C	1250	55.8	0.143	0.015	−0.03	87.6	380	120	4.62	0.25	
	CG160_16	R	1280	51.9	0.066	0.004	0.12	97.5	1900	550	4.99	0.20	
	CG160_19	C	1310	53.2	0.070	0.005	−0.03	97.0	1800	390	4.86	0.20	
	CG160_19	R	1200	52.2	0.126	0.004	0.03	89.7	2600	550	4.92	0.24	
	CG160_23	R	1220	55.7	0.112	0.011	−0.19	91.5	830	170	4.94	0.26	
										Average	4.91	0.18	
										MSWD		0.38	
	CG160_10	R	1170	47.9	0.076	0.008	0.17	96.2	890	400	5.40	0.23	
	CG160_10	C	1110	42.4	0.068	0.003	−0.07	97.3	3800	550	5.77	0.23	
Upper Merihuaca 5.49 ± 0.11	CG90_10	C	1190	57.3	0.080	0.006	−0.07	95.7	1200	250	5.27	0.26	
	CG90_10	R	1220	44.9	0.055	0.002	0.01	98.8	4200	1000	5.34	0.20	
	CG90_14	C	1070	44.3	0.065	0.005	−0.09	97.6	1100	330	5.96	0.25	

Table 1 (*continued*)

[a]Ignimbrite $^{40}Ar/^{39}Ar$ age [Ma]	Sample and crystal number	Core/rim analyses	$^{238}U/^{206}Pb$	$^{238}U/^{206}Pb$ 1 s.e.	[b] $^{207}Pb^*/^{206}Pb^*$ 1 s.e.	$^{207}Pb^*/^{206}Pb^*$ 1 s.e.	Correlation of concordia ellipses	Radiogenic %	U ppm	Th ppm	$^{206}Pb/^{238}U$ Age t [Ma]	1 sigma t [Ma]	[c] Δt [Ma]
	CG90_14	R	1250	46.8	0.057	0.003	0.03	98.6	4400	910	5.20	0.20	
	CG90_24	C	1030	40.7	0.108	0.018	−0.36	92.1	3000	3800	5.84	0.29	
	CG90_24	R	1220	44.6	0.080	0.003	0.06	95.6	3900	1200	5.13	0.19	
	CG90_2	C	1170	43.3	0.056	0.002	0.01	98.8	3400	3800	5.50	0.20	
	CG90_4	R	1200	44.2	0.056	0.004	0.09	98.7	1800	1900	5.38	0.20	
	CG90_4	C	1020	41.1	0.118	0.008	0.27	90.8	3600	940	5.86	0.26	
										Average	5.43	0.22	
										MSWD		1.70	
	CG462_1	C	1110	60.6	0.123	0.008	−0.19	90.1	580	140	5.32	0.33	
	CG462_1	R	1180	55.4	0.063	0.003	−0.01	97.8	1800	320	5.42	0.26	
	CG462_12	C	1020	46.2	0.132	0.010	0.19	89.0	920	130	5.71	0.29	
	CG462_15	C	413	24.6	0.534	0.011	−0.04	37.2	820	390	5.89	1.14	
	CG462_17	C	1100	45.8	0.175	0.008	−0.07	83.4	1100	250	4.99	0.26	
	CG462_17	R	670	36.2	0.431	0.008	−0.11	50.5	960	300	4.95	0.61	
	CG462_18	C	1190	50.1	0.071	0.008	−0.20	96.8	890	270	5.33	0.24	
	CG462_2	C	1120	51.5	0.062	0.004	0.11	97.9	1400	180	5.73	0.27	
	CG462_20	C	1220	68.9	0.075	0.005	−0.09	96.3	840	200	5.20	0.30	
	CG462_20	R	1080	47.1	0.115	0.008	0.15	91.1	1000	370	5.55	0.27	
	CG462_3	C	862	51.8	0.278	0.016	−0.23	70.2	570	180	5.34	0.51	
	CG462_4	C	1170	62.5	0.071	0.007	0.07	96.8	740	170	5.45	0.30	
	CG462_4	C	1310	65.1	0.080	0.006	−0.01	95.7	680	190	4.80	0.25	
	CG462_4	R	1110	49.6	0.137	0.007	0.01	88.3	1200	550	5.22	0.27	
	CG462_8	C	1160	64.4	0.085	0.007	0.05	95.0	660	160	5.39	0.31	
										Average	5.32	0.15	
										MSWD		0.87	
Middle Merihuaca 5.56 ± 0.15	CG482_11	C/R	1120	46.0	0.055	0.002	0.00	98.9	3300	1100	5.78	0.24	
	CG482_14	C/R	655	32.9	0.385	0.008	−0.04	56.4	2400	490	5.65	0.56	
	CG482_6	C/R	1400	134	0.075	0.006	0.38	96.3	710	520	5.53	0.44	
	CG482_9	C	1140	45.7	0.054	0.002	−0.08	99.0	2700	540	5.69	0.23	
	CG482_9	R	1120	45.7	0.054	0.003	0.01	99.0	3900	1100	5.81	0.24	
	CG482_2	C	1180	59.7	0.059	0.003	−0.08	98.4	1800	500	5.47	0.28	
	CG482_2	R	426	21.4	0.545	0.012	−0.07	35.8	1100	370	5.50	0.96	
	CG482_3	R	1230	63.6	0.054	0.004	−0.03	99.0	2200	390	5.31	0.27	
	CG482_10	C	1220	50.4	0.088	0.010	−0.33	94.6	910	640	5.06	0.23	
	CG482_10	R	1040	51.8	0.072	0.004	−0.16	96.7	910	420	6.08	0.31	
	CG482_12	C	1140	44.0	0.062	0.005	−0.09	97.9	1100	510	5.62	0.26	
	CG482_12	R	1180	48.9	0.074	0.005	−0.17	96.5	1000	410	5.37	0.25	
	CG482_14	C	741	36.0	0.347	0.011	−0.14	61.2	2200	190	5.43	0.49	
	CG482_14	R	1170	54.5	0.056	0.003	0.03	98.8	2100	190	5.55	0.26	
	CG482_3	C	1270	50.1	0.048	0.003	0.00	99.8	2500	520	5.17	0.24	
										Average	5.52	0.14	
										MSWD		0.98	
Lower Merihuaca 5.60 ± 0.20	CG476_5	C	1220	54.1	0.056	0.004	0.11	98.8	1500	430	5.30	0.25	
	CG476_5	R	1250	49.7	0.060	0.004	−0.17	98.2	1700	600	5.16	0.24	
										Average	5.23	0.34	
										MSWD		0.2	
	CG476_4	C	12.3	0.5	0.058	0.001	0.06	99.9	260	51	504	23	
	CG476_4	R	12.1	0.5	0.058	0.001	−0.02	99.9	200	45	511	24	
	CG475_10	C	1060	41.5	0.058	0.003	−0.03	98.5	1500	2400	6.03	0.28	
	CG475_10	R	1050	40.2	0.081	0.005	0.03	95.6	850	970	5.94	0.27	
	CG475_2	C/R	1120	52.9	0.063	0.006	−0.30	97.8	890	470	5.69	0.27	
	CG475_6	C	1160	45.0	0.058	0.003	−0.16	98.4	1400	320	5.57	0.26	
	CG475_6	R	1190	41.2	0.055	0.002	−0.07	98.8	2900	620	5.46	0.25	
										Average	5.72	0.23	
										MSWD		0.82	

[a] All $^{40}Ar/^{39}Ar$ ages from biotite crystals except for the CGI where an $^{40}Ar/^{39}Ar$ sanidine age is used.
[b] $^{207}Pb^*/^{206}Pb^*$ values refer to radiogenic Pb isopotes. Values for common Pb corrections taken from Sanudo-Wilhelmy and Flegal (1994).
[c] Refers to the difference between U–Pb zircon ages and the $^{40}Ar/^{39}Ar$ sanidine eruption age for that ignimbrite. Only the CGI has an associated sanidine age.

the average U-Pb age of the main zircon population (population 1) for the Cueva Negra Ignimbrite (3.73 ± 0.31 Ma; Fig. 3b). The age of the interior of this zircon crystal is within error of the average U-Pb age of the main zircon population of the underlying Real Grande Ignimbrite (4.91 ± 0.22 Ma; Fig. 3b). The interior of this crystal is therefore consistent with population 2 as described above. Crystal #13 in the Cueva Negra Ignimbrite (sample CG 519) yields an interior age of 510 ± 20 Ma and a rim age of 3.64 ± 0.54 (Fig. 2b). Again, the rim U-Pb age of this crystal is coincident (within error) with the main zircon crystallization age range of the Cueva Negra Ignimbrite (population 1), while the interior corresponds to crystallization of deposits with Late Proterozoic to Early Ordovician ages (population 3). The Blanco, Upper, and Middle Merihuaca Ignimbrites contain only zircon crystals classified as population 1. Other zircon populations could exist in these older ignimbrites, and because of the limited numbers of zircon crystals studied and uncertainties of the method, we cannot rule out the existence of multiple zircon populations.

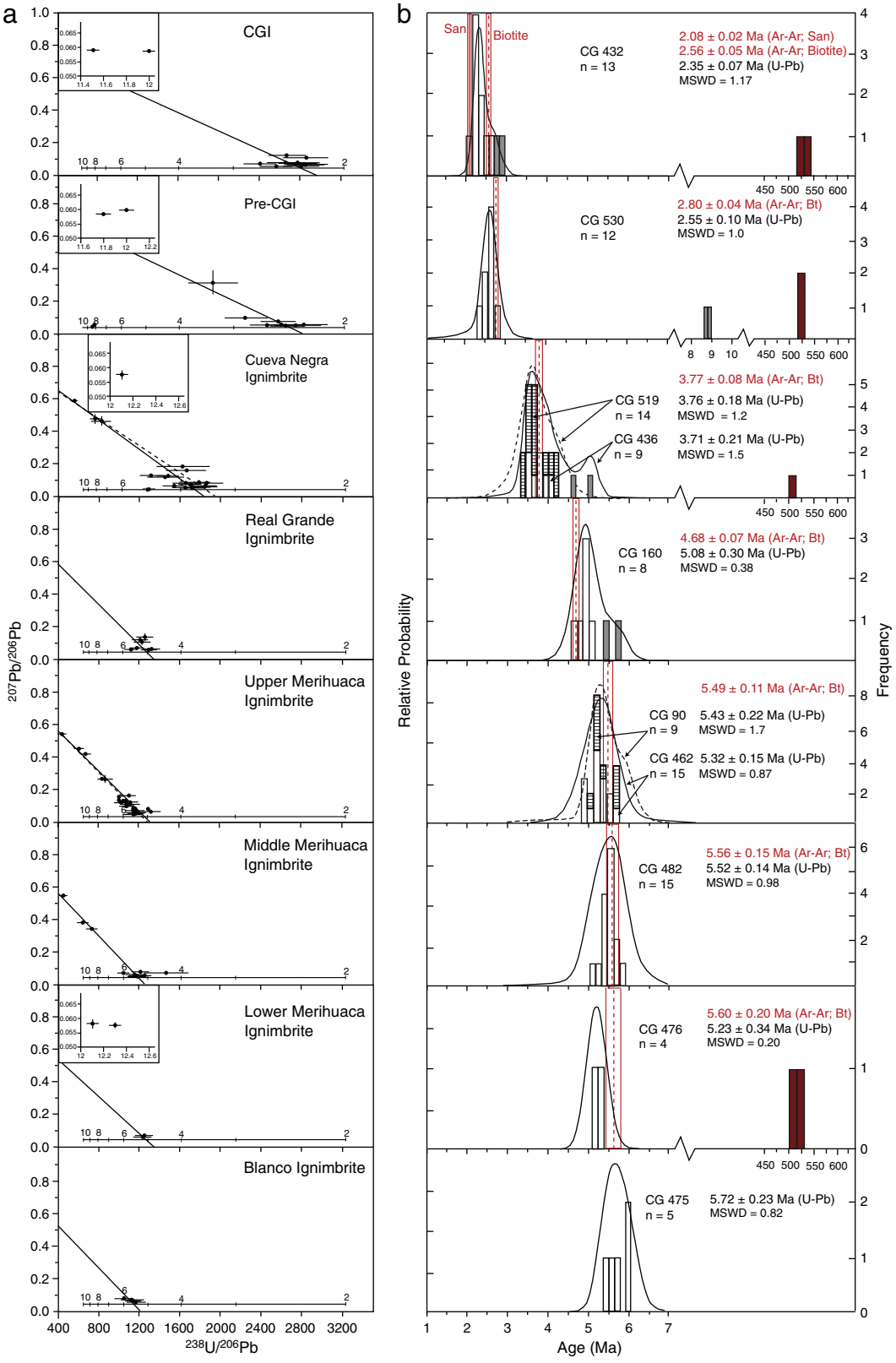

Fig. 3. (a) Tera–Wasserburg diagrams ($^{207}Pb/^{206}Pb$ vs. $^{238}U/^{206}Pb$) of zircon crystals in the Galán Ignimbrites. One-sigma error bars are shown. (b) Probability density plots and histograms (calculated with the Isoplot/Ex 3.00 software; Ludwig, 2003) for the zircon crystals analyzed in part a). Histogram bin widths are 0.15 Ma for U-Pb ages from 0–10 Ma, and 15 Ma for U-Pb ages older than 450 Ma. Further analyzed samples for the Cueva Negra and Upper Merihuaca ignimbrites are shown as bars with horizontal stripes and as dashed lines in the probability density plots. Average U-Pb zircon autocryst ages shown for each ignimbrite were calculated using the 'Weighted Average' function in Isoplot. $^{40}Ar/^{39}Ar$ ages (in red in online version, from biotite crystals except the CGI where both biotite and sanidine $^{40}Ar/^{39}Ar$ ages are presented; see Kay et al., 2011) are shown for each ignimbrite in text and lines on histograms. Inferred zircon antecrysts are shown as light gray bars and zircon xenocrysts as dark gray bars (dark red in online version) in histograms. Concordia in these diagrams account for initial disequilibrium (^{230}Th deficit; Schmitt et al., 2003a) which requires a correction of approximately +100 ka for $^{206}Pb/^{238}U$ zircon ages.

U-Pb zircon ages (in text, calculated as 'Weighted Average' ages using the Isoplot function, with individual spot analyses as open/striped histogram bars) are compared to $^{40}Ar/^{39}Ar$ ages in Fig. 3b. MSWD (Mean Square Weighted Deviates) values for the weighted average are all close to 1 (except for the Lower Merihuaca Ignimbrite where the low number of analyses accidentally resulted in a MSWD value $\ll 1$). $^{40}Ar/^{39}Ar$ ages from biotite crystals are shown for all ignimbrites (dashed lines), as well as a $^{40}Ar/^{39}Ar$ sanidine age for the CGI (solid line). The youngest individual zircon analysis for each ignimbrite is between 0.28 and 0.69 Ma (average of 0.46 ± 0.28 Ma) younger than the associated $^{40}Ar/^{39}Ar$ biotite ages (except the Real Grande Ignimbrite with a difference of 0.06 Ma). The difference between the $^{40}Ar/^{39}Ar$ sanidine age and individual U-Pb zircon spot ages for the CGI indicates zircon crystallization on average 0.26 ± 0.11 Ma and a maximum of 0.51 ± 0.1 Ma prior to eruption, (Fig. 3b; Table 1).

The relative abundances of these three distinct zircon populations in the Galán Ignimbrites suggest three distinct origins: 1) *Autocrysts* with ages within $\ll 1$ Ma of the inferred eruption age (86% of all analyses; these comprise rims and interiors); 2) *Antecrysts*[2] with ages corresponding to the dominant (type 1) zircon crystallization age peak in a previously erupted Galán ignimbrite (8% of all analyses; mostly interiors); and 3) *Xenocrysts* with basement ages (6% of all analyses; entire grains and interiors). All of the ignimbrites in the Galán stratigraphy contain dominantly autocrysts; the CGI, pre-CGI, Cueva Negra, Real Grande and Pitas Ignimbrites contain antecrysts; and the CGI, pre-CGI, Cueva Negra and Lower Merihuaca Ignimbrites have xenocrysts as well. We recognize that the relative proportions and distributions are preliminary because of the small number of individual crystals analyzed, but note their broad similarity with other studies of large-volume silicic ignimbrites (e.g., the Fish Canyon Tuff, Bachmann et al., 2007b; and the Bishop Tuff, Simon and Reid, 2005).

5. Discussion

5.1. Reliability of eruption age constraints

Minimum pre-eruptive magma residence times are estimated from the difference between $^{206}Pb/^{238}U$ zircon autocryst crystallization ages and eruption ages. Eruption ages for the Galán system determined by the Ar-Ar dating of biotite however, are problematic because they were shown to exceed those of coexisting sanidine by up to 500 ka (Hora et al., 2011). This is due to extraneous ^{40}Ar contained within biotite crystals by incomplete pre-eruptive degassing (Hora et al., 2011). $^{40}Ar/^{39}Ar$ ages from CGI biotite (Folkes et al., 2011a) are 480 ka older than those from CGI outflow sheet sanidine crystals (average 2.08 ± 0.02 Ma; Kay et al., 2011; Hora et al., 2011; and Hynek et al., 2011). This younger $^{40}Ar/^{39}Ar$ sanidine age is consistent with Rb-Sr age determinations using a combination of biotite, plagioclase and sanidine crystals in the CGI by Sparks et al. (1985). We therefore conclude that $^{40}Ar/^{39}Ar$ sanidine ages more accurately define the eruption ages of the Galán ignimbrites.

However, the absence of appreciable proportions of sanidine in all but the most recent CGI ignimbrites in the Galán stratigraphy precludes calculation of $^{40}Ar/^{39}Ar$ sanidine eruption ages for the older ignimbrites. Moreover, simple corrections based on the 480 ka difference between biotite and sanidine ages for the CGI are precluded by variable offsets between $^{40}Ar/^{39}Ar$ biotite and sanidine ages (Hora et al., 2011). In fact, one unit examined by Hora et al. (2011) *did* have concordant biotite–sanidine ages. This notwithstanding, we remain mindful that the eruption ages of the older Galán Ignimbrites could be up to ~500 ka younger than their $^{40}Ar/^{39}Ar$ biotite ages rendering comparisons between U-Pb zircon ages and $^{40}Ar/^{39}Ar$ eruption ages for the older Galán Ignimbrites approximate.

[2] Antecrysts are defined as 'phases that originate in the magma system but are not true phenocrysts' (W. Hildreth; presentation at the Penrose Conference on 'Longevity and Dynamics of Rhyolitic Magma Systems', 2001).

The youngest $^{206}Pb/^{238}U$ zircon age of the CGI (2.16 ± 0.12 Ma; Table 1) is analytically indistinguishable from the $^{40}Ar/^{39}Ar$ sanidine age (2.08 ± 0.02 Ma; Kay et al., 2011), and 0.4 Ma younger than the $^{40}Ar/^{39}Ar$ biotite age (2.56 ± 0.05 Ma) for this ignimbrite (Folkes et al., 2011a). The youngest zircon ages for the Pre-CGI, Cueva Negra, and Merihuaca Formation Ignimbrites are between 0.28 and 0.69 Ma (average of 0.46 ± 0.28 Ma) younger than the associated $^{40}Ar/^{39}Ar$ biotite ages for each ignimbrite. The youngest zircon age for the Real Grande Ignimbrite is within error of the $^{40}Ar/^{39}Ar$ biotite age. Because of the similar U-Pb ages of the youngest zircon crystals in the CGI and the $^{40}Ar/^{39}Ar$ sanidine age for the CGI, and the difference between the youngest U-Pb zircon ages and $^{40}Ar/^{39}Ar$ biotite ages in the older Galán Ignimbrites, the youngest U-Pb zircon age in each ignimbrite could be used to infer the eruption age for those Galán Ignimbrites where sanidine is absent. However, this hypothesis must be used with caution for the ignimbrites in the Galán stratigraphy where only a few crystals were analyzed (the Real Grande, Lower Merihuaca and Blanco Ignimbrites; Table 1), and the potential of ion beam overlap onto older zircon domains within crystals.

5.2. Zircon residence times and magma longevity

The zircon crystals that we have grouped as population 1 (autocrysts) within each ignimbrite exhibit a range in U-Pb ages (an average of 0.64 ± 0.26 Ma; Table 1). This range exceeds averaged uncertainties associated with individual U-Pb zircon spot analyses of autocrysts (0.27 Ma). Further, zircon crystals in the CGI that we have grouped as autocrysts yield U-Pb ages that are statistically older (0.51 ± 0.10 Ma at the maximum) than the $^{40}Ar/^{39}Ar$ sanidine eruption age (Fig. 3). In all units, zircon autocryst ages appear to form a coherent group as indicated by MSWD values close to unity with no apparent age gaps for each ignimbrite (Table 1; Fig. 3b). This suggests that zircon autocryst crystallization was continuous over several 100's ka prior to the final eruption of each ignimbrite. However, because of the small number of zircon crystals analyzed for each ignimbrite, and with their associated uncertainties, it is presently unresolved if zircon autocrysts crystallized episodically or continuously prior to eruption, and how far back this crystallization interval extends.

Correlations between repose time and volume of erupted magma can be expected because longer periods of quiescence allow larger volumes of magma to accumulate in shallow magma chambers (e.g., Smith, 1979). However, magma residence times of $>10^5$ yr are indicated by U-Th and U-Pb zircon geochronology (as reviewed by Reid, 2008; Simon et al., 2008), with erupted volumes frequently uncorrelated to pre-eruptive residence (Reid et al., 1997). We infer from U-Pb crystallization ages in zircon autocrysts of the Galán Ignimbrites, that magma residence is $>10^5$ yr (but likely $<10^6$ yr) even for the most voluminous eruptions, similar to other crystal-rich monotonous ignimbrites in the Central Andes (e.g., Schmitt et al., 2002). Such timescales are also commensurate with modeled durations of magma accumulation (e.g., Jellinek and DePaolo, 2003; de Silva and Gosnold, 2007). Conditions conducive for protracted crystallization at super-solidus temperatures are thermally buffered crystal mushes where effective crystal-melt segregation is largely inhibited, thus generating chemically homogeneous ignimbrites upon eruption (Bachmann and Bergantz, 2008). In some cases, extraction of large volumes of non-zoned crystal-poor rhyolites could be triggered by gas-driven filter pressing (Sisson and Bacon, 1999) or compaction (Bachmann and Bergantz, 2004), particularly if favorable magma chamber geometries allow segregation (e.g., Lindsay et al., 2001).

5.3. Recycled zircons in the Cerro Galán system

The presence of zircon antecrysts (population 2) that correspond to eruption and/or crystallization ages of earlier ignimbrites within the same magmatic system is first documented for the Central Andes in several of the Galán Ignimbrites (the CGI, pre-CGI, Cueva Negra,

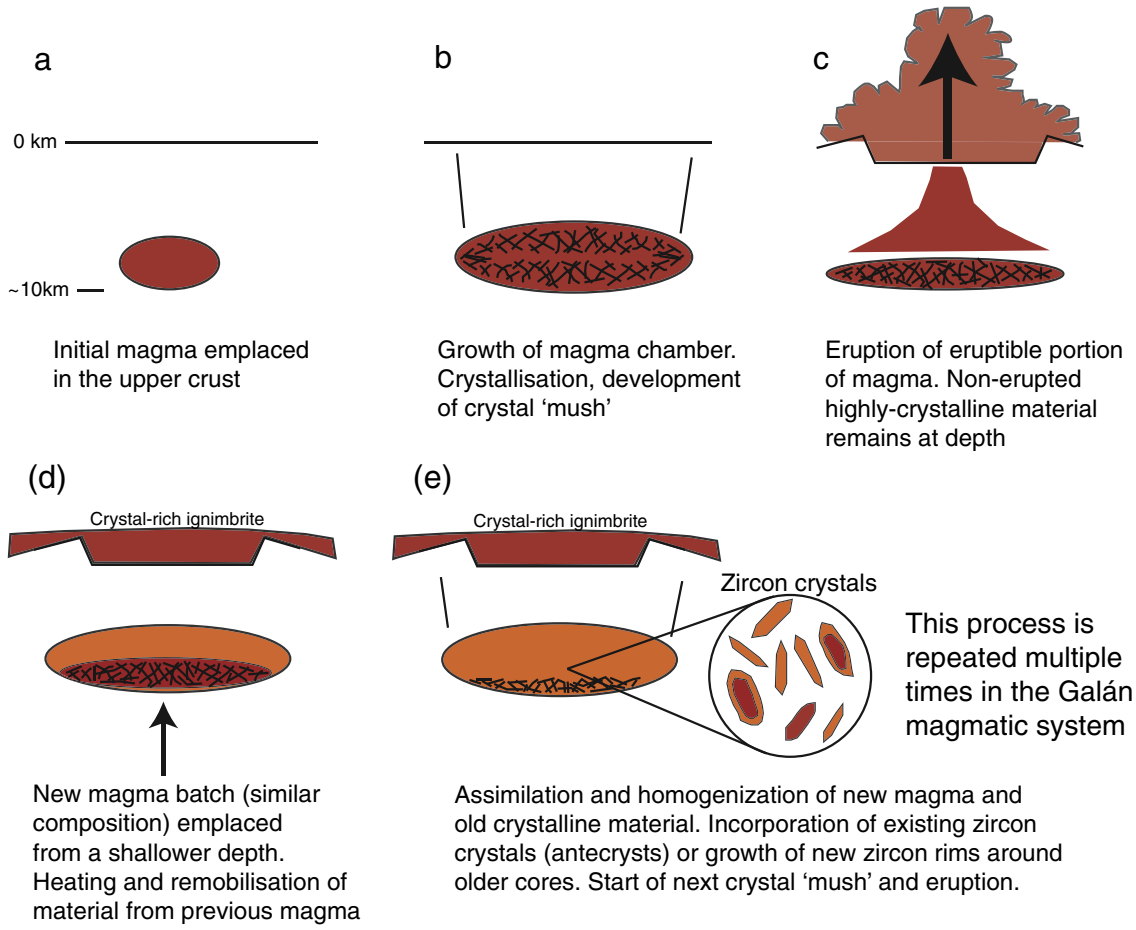

Fig. 4. Cartoon summarizing magmatic recycling suggested for the Cerro Galán magma system.

Real Grande and Upper Merihuaca Ignimbrites; Table 1) in this study. Magmatic 'recycling' of residual non-erupted, partially solidified material following an ignimbrite eruption or non-erupted pluton may represent a common process in the Galán system (Fig. 4). It is conceivable that this material cooled, either forming a crystal-mush or pluton from which crystals were remobilized during the accumulation and growth of the next batch of ignimbrite-forming magma (e.g., after underplating with hotter, less evolved magma represented by the gray pumice). The overgrowth of younger rims around antecrystic interiors could have been promoted in successive magmatic phases without resorption if compositions and temperatures remained constant. Our reconnaissance data lack evidence in CL images or U-Pb zircon ages for multiple overgrowths of new rims around older interiors, or multiple populations of antecrysts in the ignimbrites, suggesting zircon crystals only went through one period of recycling before being incorporated into the next ignimbrite eruption.

There is also rare evidence for incorporation of material into the Galán magmas with ages that predate the onset of ignimbrite eruptions in this system. The pre-CGI intracaldera deposit (CG 530) contains a single zircon crystal with ages ~2 Ma older than the date quoted for the onset of ignimbrite activity from the Galán system (Sparks et al., 1985), but close to the 9–10 Ma ages recorded for 'dacite lavas' from the Galán region by Francis et al. (1980). Although the errors of these dacite lava ages are not reported, the K-Ar methods used by these authors would likely have associated uncertainties of ± 0.5 Ma, overlapping, within error, with the U-Pb zircon ages of this CG 530 antecryst. These antecrystic ages could reflect incorporation of material from the same magma reservoir that produced these dacite lavas, generated from the earliest known phase of volcanism in the Cerro Galán region. The non-erupted solidified plutonic equivalents of these erupted lavas were then remobilized and assimilated into the magmas producing the CG 530 sample. This may represent the initiation of the magmatic system tapped by the Toconquis to the CGI eruptions in the Cerro Galán region. This observation is similar to the ~13 Ma zircons from the La Pacana caldera in the APVC (Fig. 1) for which surface volcanic equivalents have not been identified, implying the onset of felsic magmatism within the Altiplano-Puna Ignimbrite province ~3 Ma before the oldest eruptions (Schmitt et al., 2002).

Recycling of plutonic crystals is not restricted to zircon, although it is difficult to constrain the ages for major phenocryst phases. Bacon and Lowenstern (2005) reported zircon, plagioclase, and other phases in rhyodacitic lava samples pre-dating the climactic Mount Mazama eruption by ~20 ka at Crater Lake volcano that have been recycled from a known plutonic source. The preservation of mineral phases across multiple melting and crystallization events usually depends on their stability in the new melt. As the magmas that produced the Galán Ignimbrites were of very similar compositions (Folkes et al., 2011b), the main mineral phases found in the ignimbrites would have remained stable over the lifetime represented by the ignimbrite chronology. Furthermore, low temperature magmas with a rhyolitic interstitial melt, such as those in the Galán system, would tend to preserve 'granitic' mineral phases (including zircon), even if out of equilibrium, because of sluggish dissolution kinetics (Watson, 1996). Indeed, complex crystallization histories with evidence of crystal recycling are observed in preliminary CL imaging of quartz crystals in the CGI, exhibiting varying growth zonations and truncations (H. Wright, pers. comm.). The recycling of magmatic material at Cerro Galán could have been aided by the shallowing of the depth of magma storage over time (Folkes et al., 2011b). From the presence of zircon antecrysts and evidence of crystal recycling in quartz crystals, we

suggest that as each new magma batch accumulated and grew in the upper crust, it would have re-melted and remobilized non-erupted material from the previous eruption that had crystallized at slightly deeper depths (Fig. 4).

5.4. Evidence for assimilation of crustal material in the Galán magmas

The petrogenesis of the Galán magmas requires the addition of significant amounts of high $^{87}Sr/^{86}Sr$ and low $^{143}Nd/^{144}Nd$ material prior to their eruption (e.g., Francis et al., 1989). Francis et al. (1989) and Kay et al. (2011) have posited that the trace element and Sr and O isotopic signatures of the Galán magmas can be explained by subequal mixtures of enriched mantle ($^{87}Sr/^{86}Sr$ ~0.7055) and crustal ($^{87}Sr/^{86}Sr$ ~0.715–0.735) components. Folkes et al. (in review) also demonstrate that the highly elevated $\delta^{18}O_{(Quartz)}$ values (+8.8 to +9.6‰) recorded in the Galán Ignimbrites require large amounts (>40%) of high-$\delta^{18}O$, crustal material in their petrogenesis. This study provides direct evidence for the incorporation of upper crustal material into the magmas at Cerro Galán. Zircon xenocrysts in the CGI, Cueva Negra and Lower Merihuaca Ignimbrites have been dated between 539 ± 22 and 504 ± 23 Ma. These ages are consistent with basement outcrops found around the Galán caldera (Sparks et al., 1985; Hongn and Seggiaro, 2001). These outcrops likely represent crustal material that hosted the accumulating Galán magmas that were then assimilated into the growing magma chambers during each cycle. Despite the limitations in a representative sampling of zircons from individual Galán ignimbrites (cf. Dodson et al., 1988), we find that the discrepancy between isotopic indicators of crustal contamination and the abundance of zircon xenocrysts (~7% for Galán) is consistent with other continental crustal silicic magma systems such as Glass Mountain Rhyolites and the Bishop Tuff (~5% xenocrysts; Simon and Reid, 2005) and Ongatiti Ignimbrite (Taupo Volcanic Zone; ~1.3% of total analyses; Brown and Smith, 2004). This implies efficient resorption of crustal zircon during the early stages of crustal melting and assimilation.

5.5. The Galán Ignimbrites and other large-volume silicic ignimbrites

The distinction between autocrysts, antecrysts and xenocrysts, based on U-Pb and U-Th dating of zircon crystals has now been widely documented in continental silicic magma systems worldwide. This includes systems located at convergent margins (e.g., Taupo, New Zealand, Charlier et al., 2005; Crater Lake, Bacon and Lowenstern, 2005), hot-spot environments (Heise caldera, Idaho, Bindeman et al., 2007), or post-subduction to extensional environments (the Timber Mountain/Oasis Valley caldera complex, Nevada Bindeman et al., 2006; the Geysers Plutonic Complex and Cobb Mountain volcanic rocks, Schmitt et al., 2003b; and the Bandelier Tuff, New Mexico Wolff et al., 1999). The Galán ignimbrites differ from these systems in that they are dominated by less silicic rhyodacitic magmas (68–71 wt.% SiO_2) with higher crystallinities (>40 vol.%), although the residual melts are rhyolitic (Folkes et al., 2011b). The system with geological and geographical features most closely related to Galán is the La Pacana caldera (in the APVC of the central Andes, ~200–400 km north of the Cerro Galán caldera; Fig. 1). La Pacana erupted the Atana–Toconao Ignimbrite pair at ~4 Ma (sanidine Ar-Ar ages, Salisbury et al., 2010 and de Silva et al. unpublished data) with a combined volume of 2700 km^3 (DRE, Lindsay et al., 2001). The Atana Ignimbrite is the most voluminous (2500 km^3) of the pair with characteristics most similar to the Galán Ignimbrites: crystal-rich (30–40%) and rhyodacitic in composition (68–70 wt.% SiO_2). Reconnaissance U-Pb zircon dating for the Atana–Toconao Ignimbrites show evidence for protracted zircon residence whereby zircon crystallized in the La Pacana magma up to 500 ka prior to eruption (Schmitt et al., 2002). The ~13 Ma zircon ages also recorded by these authors indicate recycling and incorporation of antecrysts in the La Pacana magma that represent the early onset of the APVC system. Finally, the Toconao Ignimbrite also contains rare zircon xenocrysts with U-Pb ages dating back to ~650 Ma implying the incorporation of local basement material into the La Pacana magma.

Another compositionally similar, but older system is the Fish Canyon Tuff (FCT), which comprises ~5000 km^3 of dacitic, crystal-rich (35–50 volume% crystals; 66–68 wt.% SiO_2) magma from the San Juan Volcanic field, Colorado, erupted at ~28 Ma (e.g., Bachmann et al., 2002). Differences in $^{40}Ar/^{39}Ar$ eruption and $^{206}Pb/^{238}U$ zircon crystallization ages for the FCT magma imply a protracted zircon crystallization history of up to 300 ka (and perhaps up to 600 ka) prior to eruption (Bachmann et al., 2007b). There is also a subordinate older (~35–30 Ma) FCT zircon population (4 analyses from a total of 37) that corresponds to previous magmatic cycles in the San Juan Volcanic Field (Bachmann et al., 2007b). The FCT also contains zircon xenocrysts with much older U-Pb ages (1440–2340 Ma) derived from regional Precambrian basement (Lanphere and Baadsgaard, 2001).

Thus, magmatic recycling and crustal assimilation are common processes in many large-volume magmatic systems, but on closer inspection, differences emerge between high-silica tuffs and monotonous intermediates. Zircon longevity in crystal-rich, dacitic to rhyodacitic ignimbrites (>10^5 yr; e.g., the Cerro Galán, La Pacana and Fish Canyon Tuff examples) is more extensive compared to the high-silica, crystal-poor rhyolites (<10^5 yr, Bachmann and Bergantz, 2004; e.g., the Kos Plateau and Bishop Tuffs). The retention of zircon autocrysts and the incorporation of zircon antecrysts and xenocrysts throughout the residence time of magma in the upper crust depend strongly on the stability of zircon in a particular magma. Even large zircon crystals (>100 μm) will rapidly dissolve at magmatic temperatures >800 °C in zircon-undersaturated hydrous melts (e.g., Watson, 1996; Bacon and Lowenstern, 2005). The scarcity of zircon antecrysts or xenocrysts thus could reflect higher magma flux rates so that preexisting zircon is effectively resorbed. There is also the possibility that crystal-poor high-silica rhyolite magmas extracted from dacite or rhyodacite crystal-mushes in the upper crust are biased against incorporating antecrystic and xenocrystic material from their crystal-mush 'nurseries', although this seems unlikely for tiny zircon crystals suspended in viscous high-silica melt. Finally, differences in the geological settings may affect the presence of xenocrystic material in erupted ignimbrites. For example, in the case of the Kos Plateau Tuff, the relatively thin crust (<30 km), slow convergence rates and minor mafic magma input from the mantle associated with that 'dying' subduction zone is suggested to have precluded extensive crustal assimilation (Bachmann et al., 2007a).

6. Conclusions

$^{206}Pb/^{238}U$ zircon ages in the Galán Ignimbrites yield a variety of ages revealing growth histories and allow inferences about magma dynamics prior to eruption. Various crystal populations are identified including:

1) Autocrysts (phenocrysts too small to permit unaided visual identification) that crystallized in the final magma chambers prior to eruption. These crystals show a protracted, and perhaps, continuous range in ages several 100's ka prior to the inferred eruption ages for each ignimbrite. We suggest that magma storage and accumulation was a protracted process in the Galán system.
2) Antecrysts (phases that originate in the magma system but are not true phenocrysts) that crystallized from older magmas in the Cerro Galán system. Many of the ignimbrites contain zircon (either as whole crystals or as older cores) with ages that predate the erupted age of the host magma, but are concordant with ages of preceding eruptions. These represent recycling or scavenging of the non-erupted portions of magma from each previous eruption in the Galán stratigraphy.

3) Xenocrysts derived from material unrelated to the modern volcanic activity at Cerro Galán. There are rare examples of whole zircon crystals (or interiors of crystals) in the Galán Ignimbrites that yield Late Proterozoic to Early Ordovician ages (~540 to 500 Ma). We propose that these represent the incorporation or assimilation of 'country rock' material into the Galán magmas as they were intruded into and accumulated in the upper crust.

Similar crystal types have also been observed in other large-volume ignimbrites, although Cerro Galán is unique in that it contains them in repeated eruptions from a spatially-focused source over a long, sustained period of time (>3.5 Ma). The well-constrained stratigraphy supported by $^{40}Ar/^{39}Ar$ data (taking into account the differences in biotite $^{40}Ar/^{39}Ar$ ages vs. sanidine $^{40}Ar/^{39}Ar$ ages) has allowed the identification of zircon antecrysts within ignimbrites that yield U-Pb zircon ages that are similar to the peak-crystallization ages in each preceding ignimbrite respectively. We suggest that magma dynamics and zircon crystallization histories (protracted magma residence and the incorporation of non-erupted older plutonic and country rock material) remained invariant over the lifetime of the Galán system. This is consistent with thermal and compositional buffering in long-lived crystal mushes accumulating in the upper crust that are maintained by protracted (>10^5 yr; e.g., Bachmann and Bergantz, 2008) addition or recharge of new magma batches.

Acknowledgments

This research was funded by an Australian Research Council Discovery Program Grant DP0663560 to the research team led by R. Cas. The SIMS analytical work was supported by NSF grant number 0838536 to S. de Silva and A. Schmitt. We thank Dr. H. Wright (now at USGS Menlo Park) and the MONVOLC group at Monash University for constructive discussions of this work. B. Pullen is thanked for his assistance in the extraction of zircon crystals from bulk-rock samples. Insightful and comprehensive reviews by journal reviewers Mary Reid and Charles Bacon are much appreciated and significantly improved this manuscript.

References

Bachmann, O., Bergantz, G.W., 2004. On the origin of crystal-poor rhyolites: extracted from batholithic crystal mushes. Journal of Petrology 45, 1565–1582.
Bachmann, O., Bergantz, G.W., 2008. Deciphering magma chamber dynamics from styles of compositional zoning in large silicic ash flow sheets. Reviews in Mineralogy and Geochemistry 69, 651–674.
Bachmann, O., Dungan, M.A., Lipman, P.W., 2002. The Fish Canyon magma body, San Juan volcanic field, Colorado: rejuvenation and eruption of an upper-crustal batholith. Journal of Petrology 43, 1469–1503.
Bachmann, O., Charlier, B., Lowenstern, J., 2007a. Zircon crystallization and recycling in the magma chamber of the rhyolitic Kos Plateau Tuff (Aegean Arc). Geology 35 (1), 73–76.
Bachmann, O., Oberli, F., Dungan, M., Meier, M., Mundil, R., Fischer, H., 2007b. $^{40}Ar/^{39}Ar$ and U-Pb dating of the Fish Canyon magmatic system, San Juan Volcanic field, Colorado: evidence for an extended crystallization history. Chemical Geology 236, 134–166.
Bacon, C.R., Lowenstern, J.B., 2005. Late Pleistocene granodiorite source for recycled zircon and phenocrysts in rhyodacite lava at Crater Lake, Oregon. Earth and Planetary Science Letters 233, 277–293.
Bindeman, I., Schmitt, A., Valley, J., 2006. U-Pb zircon geochronology of silcic tuffs from the Timber Mountain/Oasis Valley caldera complex, Nevada: rapid generation of large volume magmas by shallow-level remelting. Contributions to Mineralogy and Petrology 152 (6), 649–665.
Bindeman, I., Watts, K., Schmitt, A., Morgan, D., Shanks, P., 2007. Voluminous low $\delta^{18}O$ magmas in the late Miocene Heise volcanic field, Idaho: implications for the fate of Yellowstone hotspot calderas. Geology 35 (11), 1019–1022.
Bindeman, I.N., Fu, B., Kita, N.T., Valley, J.W., 2008. Origin and evolution of silicic magmatism at Yellowstone based on ion microprobe analysis of isotopically zoned zircons. Journal of Petrology 49, 163–193.
Blundy, J., Wood, B., 2003. Mineral-melt partitioning of uranium, thorium, and their daughters. In: Bourdon, B., Henderson, G.M., Lundstrom, C.C., Turner, S.P. (Eds.), U-Series Geochemistry: Reviews in Mineralogy and Geochemistry, 52, pp. 59–123.
Brown, S.J.A., Fletcher, I.R., 1999. SHRIMP U-Pb dating of the preeruption growth history of zircons from the 340 ka Whakamaru Ignimbrite, New Zealand: evidence for >250 k.y. magma residence times. Geology 27, 1035–1038.
Brown, S., Smith, R., 2004. Crystallisation history and crustal inheritance in a large silicic magma system: $^{206}Pb/^{238}U$ ion probe dating of zircons from the 1.2 Ma Ongatiti ignimbrite, Taupo Volcanic Zone. Journal of Volcanology and Geothermal Research 135, 247–257.
Charlier, B.L.A., Wilson, C.J.N., Lowenstern, J.B., Blake, S., Van Calsteren, P.W., Davidson, J.P., 2005. Magma generation at a large, hyperactive silicic volcano (Taupo, New Zealand) revealed by U-Th and U-Pb systematics in zircons. Journal of Petrology 46 (1), 3–32.
Charlier, B.L.A., Bachmann, O., Davidson, J.P., Dungan, M.A., Morgan, D.J., 2007. The upper crustal evolution of a large silicic magma body: evidence from crystal-scale rb-sr isotopic heterogeneities in the Fish Canyon Magmatic System, Colorado. Journal of Petrology 48 (10), 1875–1894.
Cherniak, D., Watson, E., 2003. Diffusion in zircon. In: Hanchar, J., Hoskin, P. (Eds.), Zircon. The Mineralogical Society of America, Washington, pp. 113–143.
Compston, W., Williams, I.S., Meyer, C., 1984. U-Pb geochronology of zircons from lunar breccia 73217 using a sensitive high mass-resolution ion microprobe. Journal of Geophysical Research Supplement 89, B525–B534.
de Silva, S., 1989a. Geochronology and stratigraphy of the ignimbrites from the 21°30′S to 23°30′S portion of the Central Andes of northern Chile. Journal of Volcanology and Geothermal Research 37, 93–131.
de Silva, S.L., 1989b. Altiplano-Puna volcanic complex of the Central Andes. Geology 17, 1102–1106.
de Silva, S.L., 1991. Zonations in silicic magma chambers—insights from Central Andean ignimbrites. Geological Society of America Special Paper 265, 217–232.
de Silva, S.L., Francis, P.W., 1989. Correlation of large ignimbrites; two case studies from the Central Andes of northern Chile. Journal of Volcanology and Geothermal Research 37, 133–149.
de Silva, S.L., Gosnold, W.D., 2007. Episodic construction of batholiths: insights from the spatiotemporal development of an ignimbrite flare-up. Journal of Volcanology and Geothermal Research 167, 320–335.
de Silva, S.L., Wolff, J.A., 1995. Zoned magma chambers: the influence of magma chamber geometry on sidewall convective fractionation. Journal of Volcanology and Geothermal Research 65, 111–118.
Dodson, M., Compston, W., Williams, I., Wilson, J., 1988. A search for ancient detrital zircons in Zimbabwean sediments. Journal of the Geological Society 145, 977–983.
Folkes, C.B., Wright, H.M., Cas, R.A.F., de Silva, S.L., Lesti, C., Viramonte, J.G., 2011a. A re-appraisal of the stratigraphy and volcanology of the Cerro Galan volcanic system. NW Argentina. Bulletin of Volcanology. doi:10.1007/s00445-011-0459-y.
Folkes, C.B., de Silva, S.L., Wright, H.M. and Cas, R.A.F., 2011b. Geochemical homogeneity of a long-lived, large silicic system; evidence from the Cerro Galan caldera, NW Argentina. Bulletin of Volcanology. doi:10.1007/s00445-011-0511-y.
Folkes, C., de Silva, S., Bindeman, I. and Cas, R., in review. Tectonic setting and climate determine the geochemistry of supervolcanic magmas: new $\delta^{18}O$ data from the central Andes. Geochemistry, Geophysics, Geosystems.
Francis, P.W., Thorpe, R.S., Moorbath, S., Kretschmar, G.A., Hammill, M., 1980. Strontium isotope evidence for crustal contamination of calc-alkaline volcanic rocks from Cerro Galan, northwest Argentina. Earth and Planetary Science Letters 48, 256–267.
Francis, P.W., Sparks, R.S.J., Hawkesworth, C.J., Thorpe, R.S., Pyle, D.M., Tait, S.R., Mantovani, M.S., McDermott, F., 1989. Petrology and geochemistry of volcanic rocks of the Cerro Galan caldera, northwest Argentina. Geological Magazine 126 (5), 515–547.
Guzman, S., Petrinovic, I., 2010. The Luingo caldera: the south-easternmost collapse caldera in the Altiplano-Puna plateau, NW Argentina. Journal of Volcanology and Geothermal Research 194, 174–188.
Hildreth, W., 1981. Gradients in silicic magma chambers: implications for lithospheric magmatism. Journal of Geophysical Research 86, 10153–10192.
Hongn, F.D., Seggiaro, R.E., 2001. Hoja Geológica 2566-III, Cachi. Provincias de Salta y Catamarca, Programa Nacional de Cartas Geológicas de la República Argentina: Buenos Aires, Segemar, p. 87.
Hora, J.M., Singer, B.S., Jicha, B.R., Beard, B.L., Johnson, C.M., de Silva, S., Salisbury, M., 2011. Volcanic biotite-sanidine $^{40}Ar/^{39}Ar$ age discordances reflect Ar partitioning and pre-eruption closure in biotite. Geology 38 (10), 923–926.
Hynek, S.A., Brown, F.H., Fernandez, D.P., 2011. A rapid method for hand picking potassium-rich feldspar from silicic tephra. Quaternary Geology 6, 285–288.
Jellinek, A., DePaolo, D., 2003. A model for the origin of large silicic magma chambers: precursors of caldera-forming eruptions. Bulletin of Volcanology 65, 363–381.
Kay, S.M., Coira, B., 2009. Shallowing and steepening subduction zones, continental lithospheric loss, magmatism and crustal flow under the central Andean Altiplano-Puna plateau. In: Kay, S.M., Ramos, V.A., Dickinson, W.R. (Eds.), Backbone of the Americas: Shallow Subduction, Plateau Uplift and Ridge and Terrane Collision: Geological Society of America Memoir, 204, pp. 229–259.
Kay, S.M., Coira, B., Woerner, G., Kay, R.W., Singer, B.S., 2011. Geochemical, isotopic and single crystal $^{40}Ar/^{39}Ar$ age constraints on the evolution of the Cerro Galan Ignimbrites. Bulletin of Volcanology. doi:10.1007/s00445-010-0410-7.
Lanphere, M.A., Baadsgaard, H., 2001. Precise K-Ar, $^{40}Ar/^{39}Ar$, Rb-Sr, U/Pb mineral ages from the 27.5 Ma Fish Canyon Tuff reference standard. Chemical Geology 175, 653–671.
Lindsay, J.M., Schmitt, A.K., Trumbull, R.B., de Silva, S.L., Siebel, W., Emmermann, R., 2001. Magmatic evolution of the La Pacana Caldera System, Central Andes, Chile: compositional variation of two cogenetic, large-volume felsic ignimbrites. Journal of Petrology 42 (3), 459–486.
Lipman, P.W., 1984. The roots of ash flow calderas in western north America: windows into the tops of granitic batholiths. Journal of Geophysical Research 89 (B10), 8801–8841.
Ludwig, K., 2003. User's Manual for Isoplot 3.00. A Geochronological Toolkit for Microsoft Excel. Berkeley Geochronology Center, Special Publication No. 4a, Berkeley, California.

Mahood, G., Hildreth, W., 1983. Large partition coefficients for trace elements in high-silica rhyolites. Geochimica et Cosmochimica Acta 47, 11–30.
Maughan, L.L., Christiansen, E.H., Best, M.G., Gromme, C.S., Deino, A.L., Tingey, D.G., 2002. The Oligocene Lund Tuff, Great Basin, USA: a very large volume monotonous intermediate. Journal of Volcanology and Geothermal Research 113, 129–157.
Paces, J.B., Miller, J.D., 1993. Precise U-Pb ages of Duluth Complex and related mafic intrusions, northeastern Minnesota; geochronological insights to physical, petrogenetic, paleomagnetic, and tectonomagmatic processes associated with the 1.1 Ga Midcontinent Rift System. Journal of Geophysical Research 98, 13997–14013.
Reid, M., 2008. How long does it take to supersize an eruption? Elements 4, 23–28.
Reid, M., Coath, C., 2000. In situ U-Pb ages of zircons from the Bishop Tuff; no evidence for long crystal residence times. Geology 28 (5), 443–446.
Reid, M., Coath, C., Harrison, T., McKeegan, K., 1997. Prolonged residence times for the youngest rhyolites associated with Long Valley Caldera: ^{230}Th-^{238}U ion microprobe dating of young zircons. Earth and Planetary Science Letters 150, 27–39.
Reid, M., Vazquez, J., Schmitt, A., 2011. Zircon-scale insights into the history of a supervolcano, Bishop Tuff, Long Valley, California, with implications for the Ti-in-zircon geothermometer. Contributions to Mineralogy and Petrology 161 (2), 293–311.
Salisbury, M.J., Jicha, B.R., de Silva, S.L., Singer, B.S., Jimenez, N.C., Ort, M.H., 2010. ^{40}Ar/^{39}Ar chronostratigraphy of Altiplano-Puna volcanic complex ignimbrites reveals the development of a major magmatic province. Geological Society of America Bulletin. doi:10.1130/B30280.1.
Sanudo-Wilhelmy, S., Flegal, A., 1994. Temporal variations in lead concentrations and isotopic composition in the Southern California Bight. Geochimica et Cosmochimica Acta 58 (15), 3315–3320.
Schmitt, A., 2011. Uranium series accessory crystal dating of magmatic processes. Annual Review of Earth and Planetary Sciences 39, 321–349.
Schmitt, A.K., Lindsay, J.M., de Silva, S., Trumbull, R.B., 2002. U-Pb zircon chronostratigraphy of early-Pliocene ignimbrites from La Pacana, north Chile: implications for the formation of stratified magma chambers. Journal of Volcanology and Geothermal Research 120, 43–53.
Schmitt, A., Grove, M., Harrison, T., Lovera, O., Hulen, J., Walters, M., 2003a. The Geysers-Cobb Mountain Magma System, California (Part 1): U-Pb zircon ages of volcanic rocks, conditions of zircon crystallization and magma residence times. Geochimica et Cosmochimica Acta 67 (18), 3423–3442.
Schmitt, A., Grove, M., Harrison, T., Lovera, O., Hulen, J., Walters, M., 2003b. The Geysers-Cobb Mountain Magma system, California (Part 2): timescales of pluton emplacement and implications for its thermal history. Geochimica et Cosmochimica Acta 67 (18), 3443–3458.
Simon, J., Reid, M., 2005. The pace of rhyolite differentiation and storage in an "archetypical" silicic magma system, Long Valley, California. Earth and Planetary Science Letters 235 (1–2), 123–140.
Simon, J., Renne, P., Mundil, R., 2008. Implications of pre-eruptive magmatic histories of zircons for U-Pb geochronology of silicic extrusions. Earth and Planetary Science Letters 266 (1–2), 182–194.
Sisson, T., Bacon, C., 1999. Gas-driven filter pressing in magmas. Geology 27 (7), 613–616.
Smith, R.L., 1979. Ash-flow magmatism. Geological Society of America Special Paper 180, 5–27.
Sparks, R.S.J., Francis, P.W., Hamer, R.D., Pankhurst, R.J., O'Callaghan, L.O., Thorpe, R.S., Page, R.N., 1985. Ignimbrites of the Cerro Galan caldera, NW Argentina. Journal of Volcanology and Geothermal Research 24, 205–248.
Watson, E., 1996. Dissolution, growth and survival of zircons during crustal fusion: kinetic principles, geological models and implications for isotopic inheritence. Geological Society of America Special Paper 315, 43–56.
White, S., Crisp, J., Spera, F., 2006. Long-term volumetric eruption rates and magma budgets. Geochemistry, Geophysics, Geosystems 7, Q03010. doi:10.1029/02005GC001002.
Whitney, J.A., Stormer, J.C., Jr., 1985. Mineralogy, petrology, and magmatic conditions from the Fish Canyon Tuff, central San Juan Volcanic Field, Colorado. Journal of Petrology 26, 726–762.
Wiedenbeck, M., Roddick, J.C., Spiegel, W., 1995. Three natural zircon standards for U-Th-Pb, Lu-Hf, trace element and REE analyses. Geostandards Newsletter 91, 1–23.
Wilson, C.J.N., Charlier, B.L.A., 2009. Rapid rates of magma generation at contemporaneous magma systems, Taupo Volcano, New Zealand: insights from U-Th model-age spectra in zircons. Journal of Petrology 50 (5), 875–907.
Wolff, J.A., Ramos, F.C., Davidson, J.P., 1999. Sr isotope disequilibrium during differentiation of the Bandelier Tuff: constraints on the crystallization of a large rhyolitic magma chamber. Geology 27, 495–498.
Wright, H.M.N., Folkes, C.B., Cas, R.A.F., Cashman, K.V., 2011. Heterogeneous pumice populations in the 2.08 Ma Cerro Galan ignimbrite: implications for magma recharge and ascent preceding a large volume silicic eruption. Bulletin of Volcanology. doi:10.1007/s00445-011-0525-5.